

Dual mode signaling responses of a rhodamine based probe and on its immobilization onto silica gel surface for specific mercury ion detection

Ajoy Pal and Bamaprasad Bag*

Colloids and Materials Chemistry Department, Academy of Scientific and Innovative Research, CSIR-Institute of Minerals and Materials Technology, P.O.: R.R.L., Bhubaneswar-751 013, Odisha, India. Fax: (+ 91) 674 258 1637; Tel: (+ 91) 674 237 9254, Email: bpbag@immt.res.in

Electronic Supplementary Information

Fig. S1-S3	¹ H, ¹³ C-NMR and ESI-MS spectra of 2	SP2-SP3
Table ST1	Selected non-bonded distances(Å), angles(°), torsion(°) of 2	SP3
Fig. S4-S9	Absorption and fluorescence spectral pattern of 2 in MeCN-H ₂ O (1:1 v/v)	SP4-SP7
Fig. S10-S16	FT-IR, FESEM, EDS, particle size analysis, Surface area determination, TGA and powder X-ray characterization of SiR-1	SP7-SP11
Table ST2	Parameters of Powder XRD analysis of SiG , SiR-1 and (SiR-1)-Hg(II) complex	SP10
Fig. S17-S20	Absorption and fluorescence spectral pattern of SiR-1 in aqueous medium	SP12-SP13

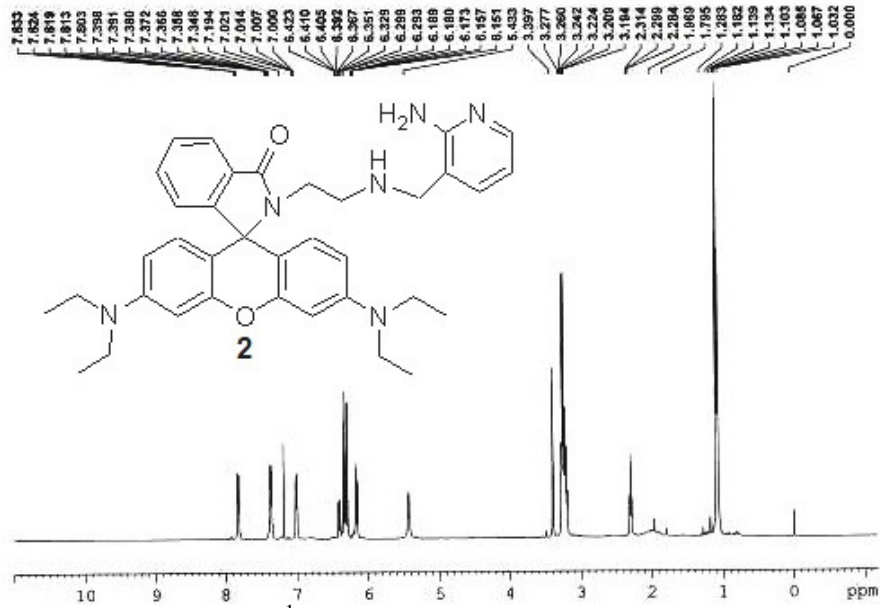


Fig. S1: ^1H -NMR spectrum of **2** in CDCl_3

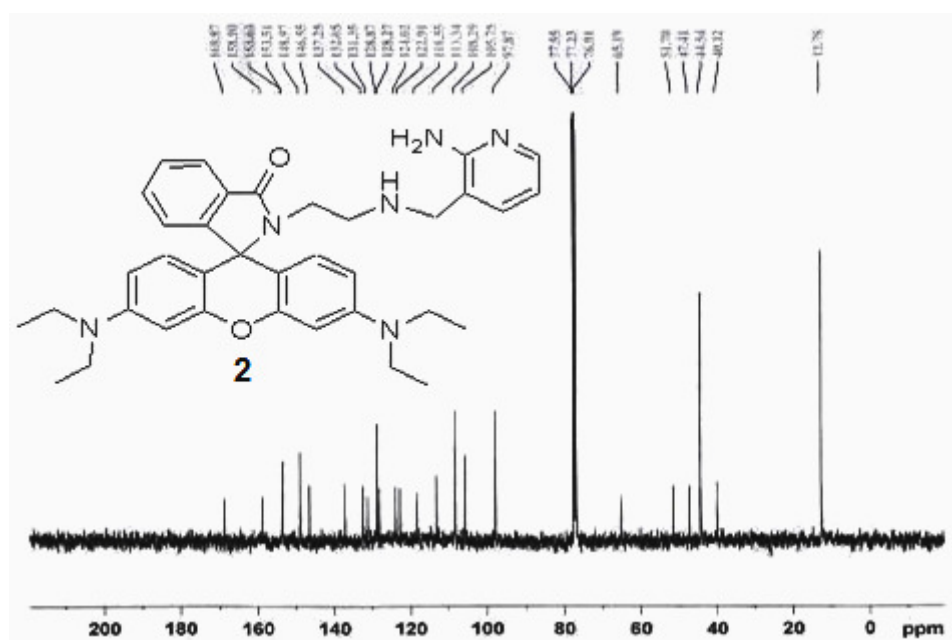


Fig. S2: ^{13}C -NMR spectrum of **2** in CDCl_3

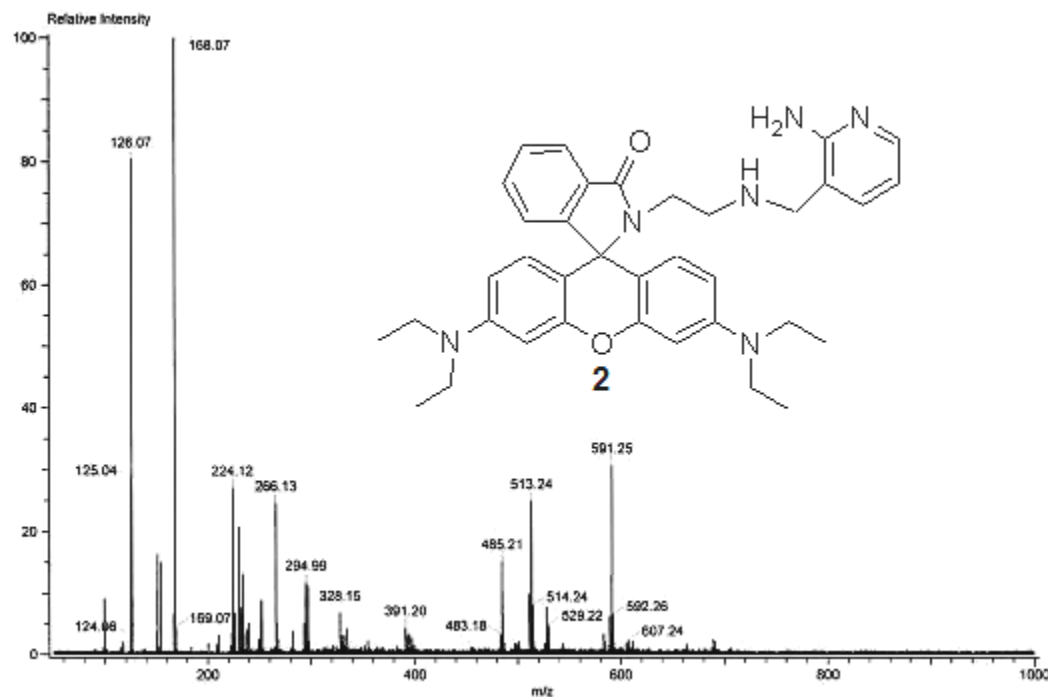


Fig. S3: ESI-MS spectrum of **2**

Table ST1: Selected non-bonded distances(Å), angles(°), torsion(°) of **2**.

Bonded/ non-bonded distances	Value(Å)	Angles/torsion angles	Value(°)
N ₅N ₆	3.001	∠C ₁₀ -C ₉ -C ₁₄	110.85
N ₄N ₅	2.773	∠C ₁₂ -C ₉ -N ₃	112.26
N ₅O ₂	6.130	∠C ₁₄ -C ₉ -N ₃	99.95
N ₅N ₃	5.979	∠C ₁₂ -C ₉ -C ₁₀	110.60
N ₃N ₄	3.707	∠O ₁ -C ₉ -C ₁₄ -C ₁₇	150.75
N ₄O ₂	4.485	∠C ₃₄ -C ₃₂ -C ₉ -O ₁	100.70
N ₃O ₂	2.296	∠C ₃₄ -C ₃₂ -C ₁₉ -C ₁₆	-166.98
N ₁C ₃	1.384		
N ₂C ₇	1.382		
C ₂₀N ₃	1.360		
C ₉N ₃	1.498		

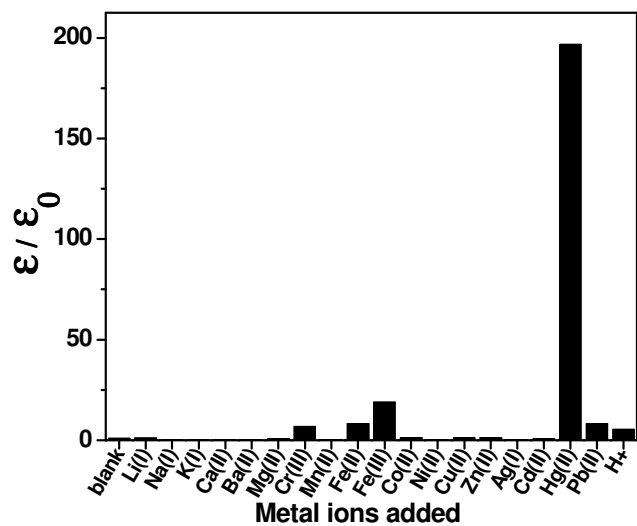


Fig. S4: Absorption enhancement factors in **2** in presence of various metal ions in MeCN-H₂O(1:1 v/v) medium. [2] = 1×10⁻⁵M, [M(I/II)] = 2×10⁻⁴M.

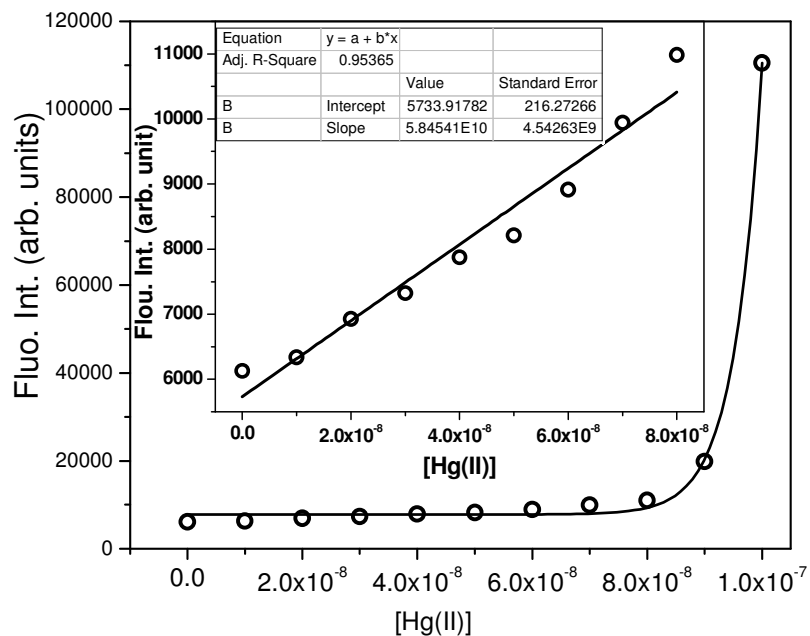


Fig. S5: Fluorescence spectral responses of **2** as a function of added Hg(II) ion concentration in MeCN-H₂O(1:1 v/v) medium; [2] = 0.1μM, λ_{ex} = 500 nm, em. and ex. b. p. = 5nm, RT. (Inset) linear regression to the plot of change in fluorescence intensity against Hg(II) concentration for determination of limit of detection.

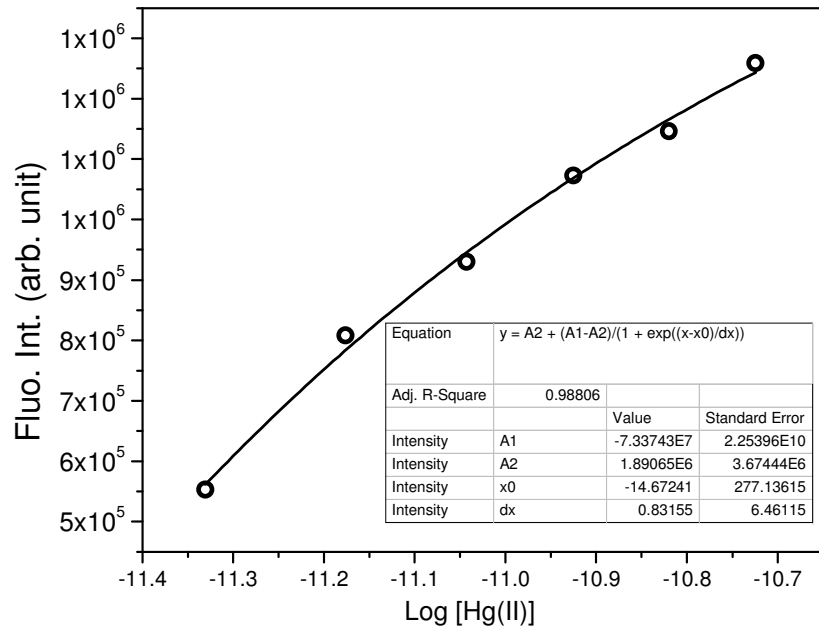


Fig. S6: Plot of change in fluorescence intensity in **2** as a function of $\log[\text{Hg(II)}]$ for determination of association constant(K_a) in **2**-Hg(II) complex. $[\mathbf{2}] = 1\mu\text{M}$, $\lambda_{\text{ex}} = 500\text{ nm}$, em. and ex. b. p. = 5nm, RT.

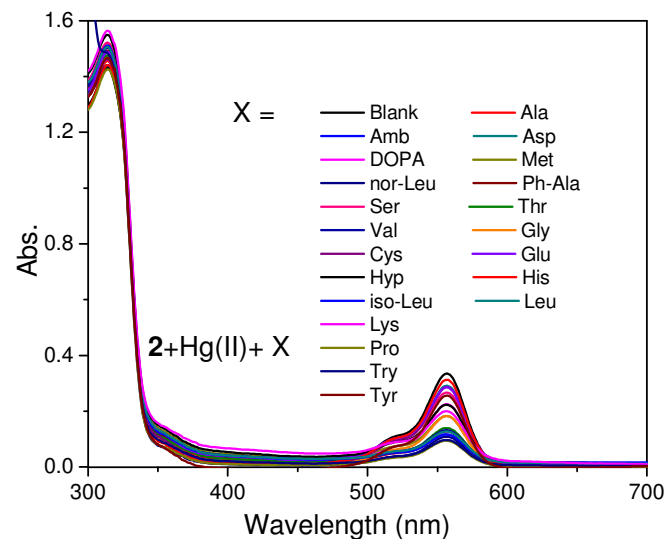


Fig. S7: Absorption spectral pattern of in-situ **2**-Hg(II) complex (addition of Hg(II) ion (10eq.) with **2** (1eq.) upon addition of (100 eq.) different amino acids in MeCN-H₂O (1:1 v/v).

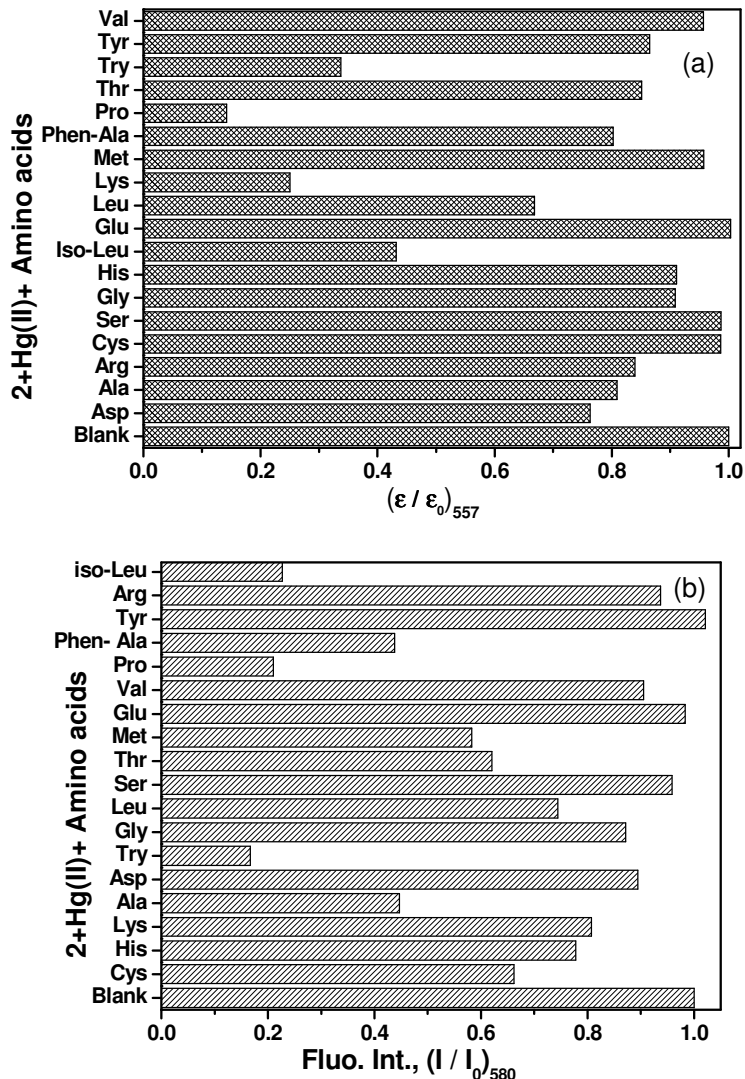


Fig. S8: Normalized absorption (a) and fluorescence(b) spectral responses of in-situ **2**-Hg(II) complex (addition of Hg(II) ion (10eq.) with **2** (1eq.) upon addition of (100 eq.) different amino acids in MeCN-H₂O (1:1 v/v).

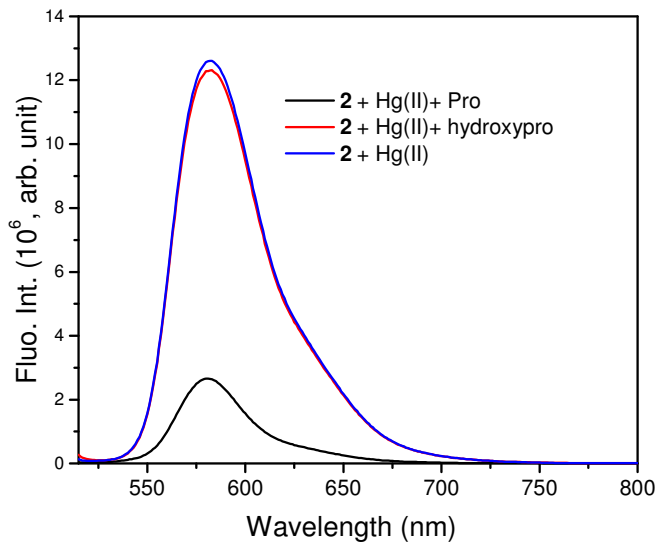


Fig. S9: Fluorescence spectra of **2-Hg(II)** upon addition of **L-Pro** and **Hyp** (hydroxyproline) in MeCN-H₂O (1:1 v/v), [2]= 1 μ M, [Hg(II)]= 10 μ M, [L-pro/hyp]= 50 μ M, $\lambda_{\text{ex}}= 500$ nm, em. and ex. b. p. = 5nm, RT.

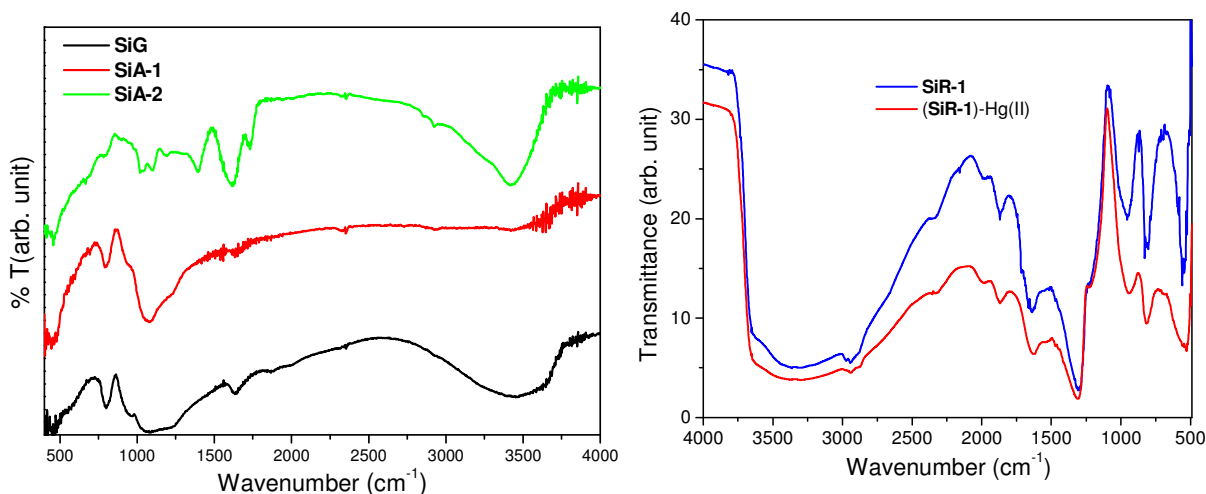


Fig. S10: FT-IR spectra of **SiG**, **SiA-1**, **SiA-2**, **SiR-1** and **(SiR-1)-Hg(II)** complex for comparison.

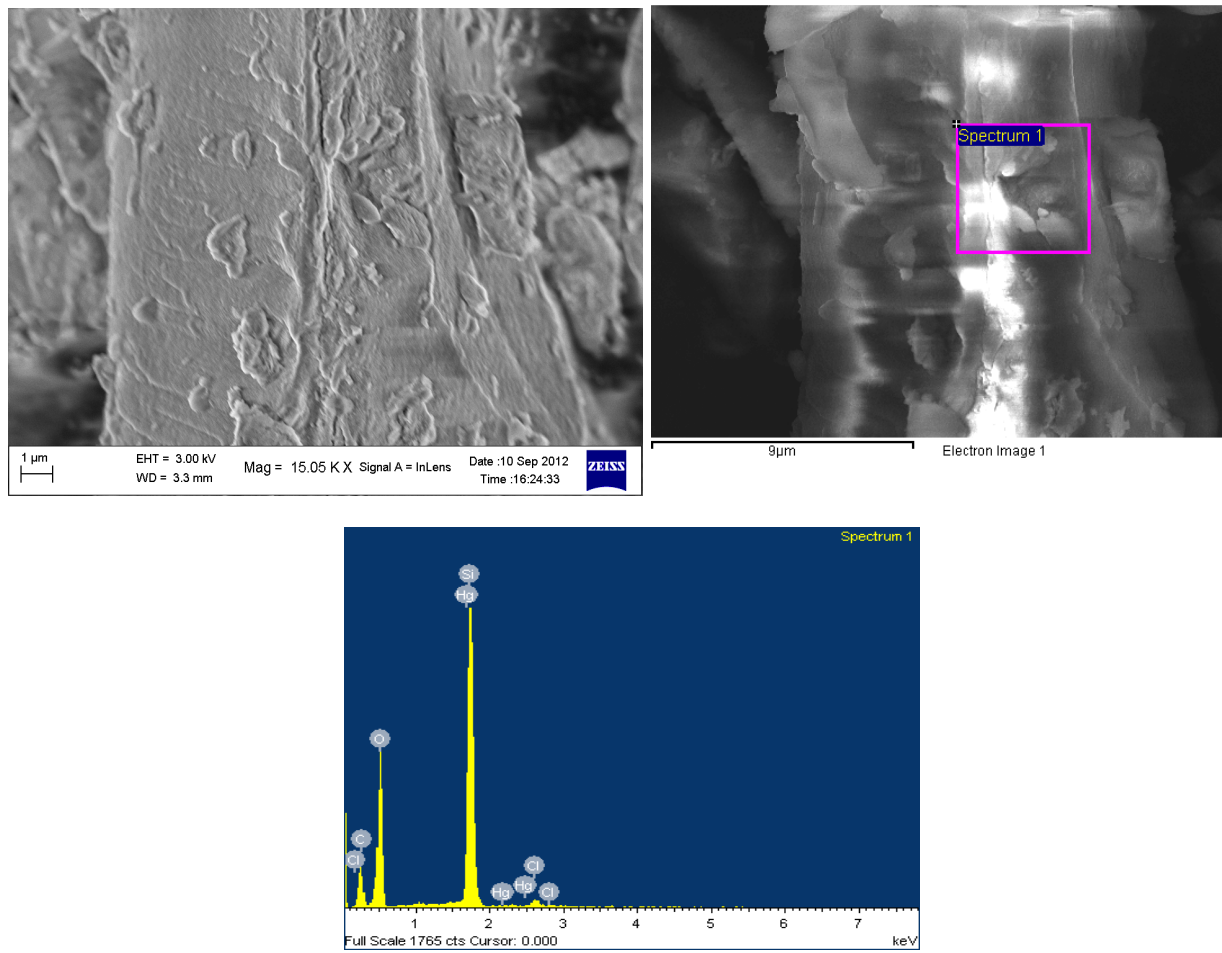


Fig. S11: FESEM image of (SiR-1)-Hg(II) complex and corresponding EDS profile.

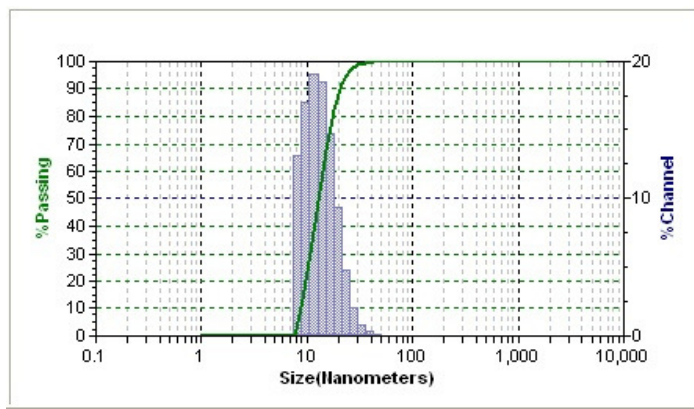


Fig. S12: Particle size distribution pattern of agglomerated probe **2** in MeCN-H₂O (1:1 v/v) medium.

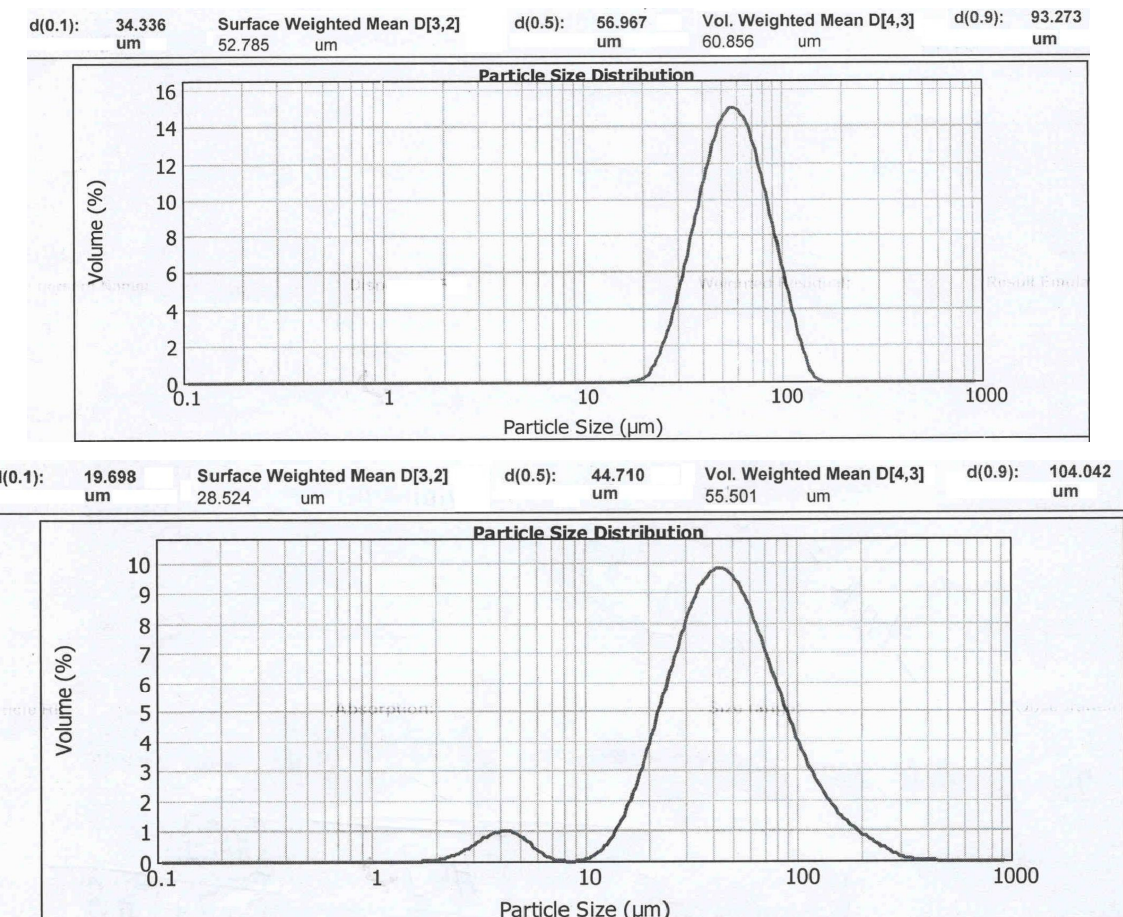


Fig. S13: Particle size distribution pattern of agglomerated **SiR-1** and **(SiR-1)-Hg(II)** complex with water as dispersant.

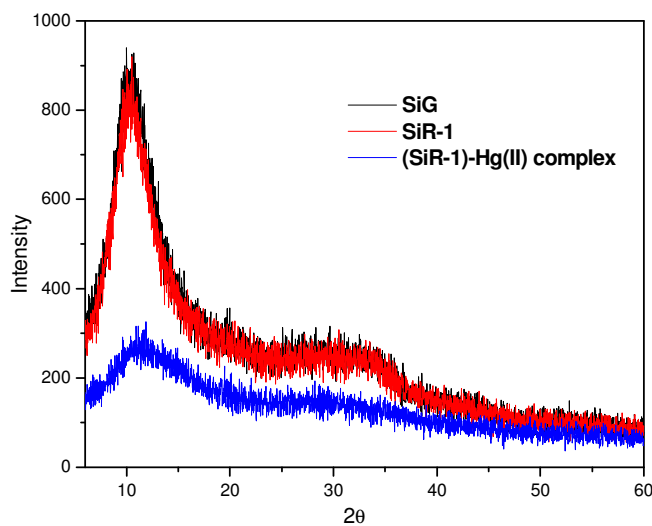


Fig. S14: Powder X-ray diffraction pattern of **SiG**, **SiR-1** and **(SiR-1)-Hg(II)** complex.

Table S2: Parameters of Powder XRD analysis of **SiG**, **SiR-1** and **(SiR-1)-Hg(II)** complex.

Sample	Pos. [°2Th.]	Height [cts]	FWHM [°2Th.]	d-spacing [Å]	Rel. Int. [%]
SiG	10.3118	24.15	0.2583	4.14714	100.00
SiR-1	10.3710	24.45	0.6136	3.92405	100.00
(SiR-1)-Hg(II)	10.7885	2.06	1.6520	3.77263	100.00

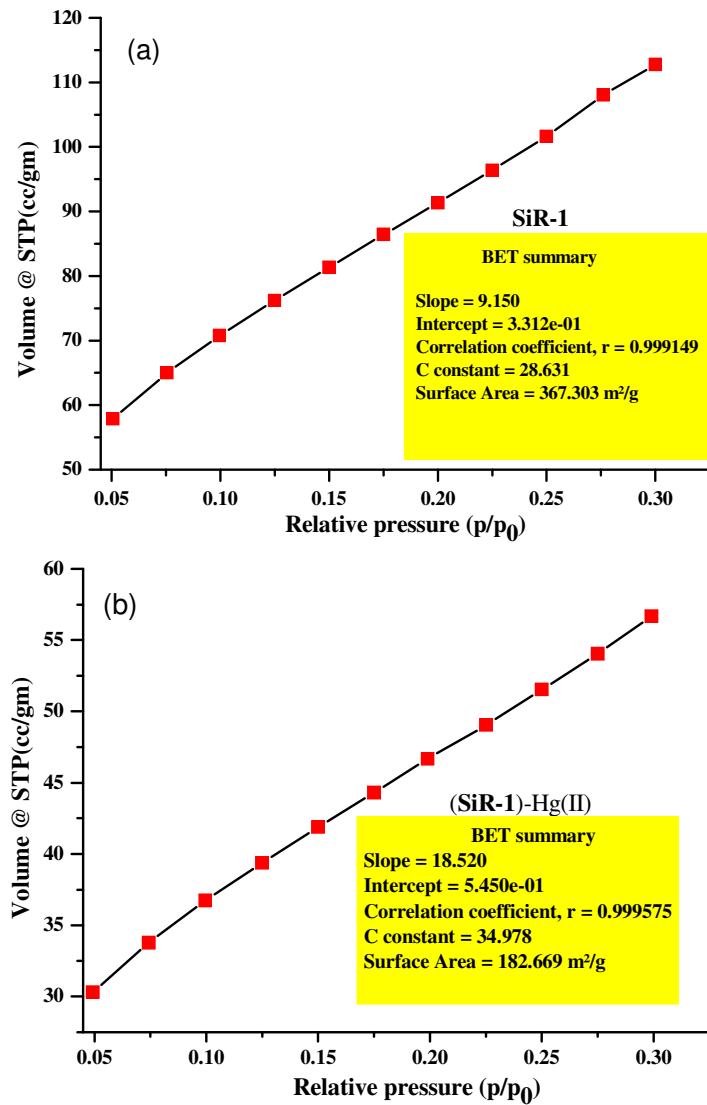


Fig. S15: Nitrogen isotherms of **SiR-1** and **(SiR-1)-Hg(II)** complex for determination of BET surface area.

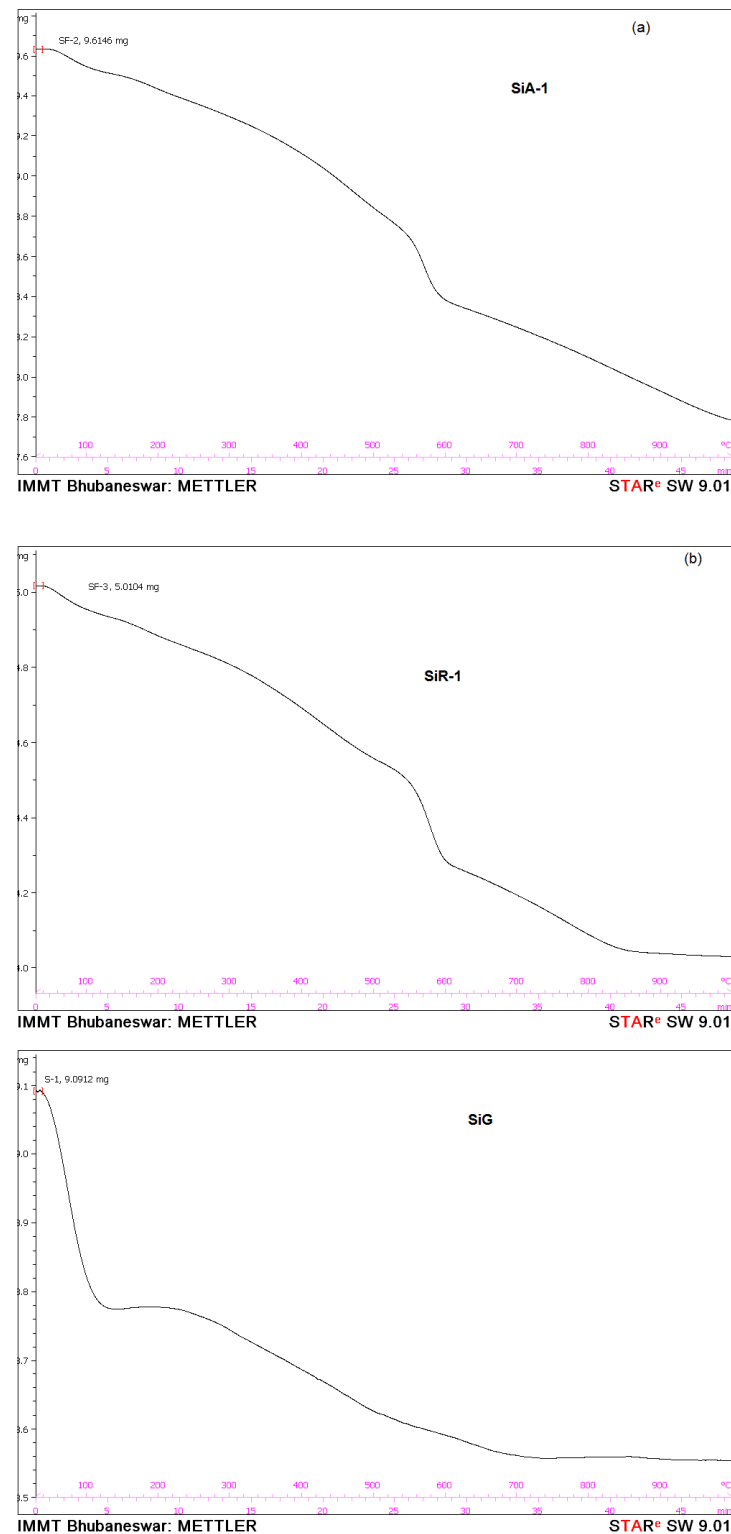


Fig. S16: TGA plots of (a) **SiA-1**, (b) **SiR-1** and (c) **SiG** for comparison.

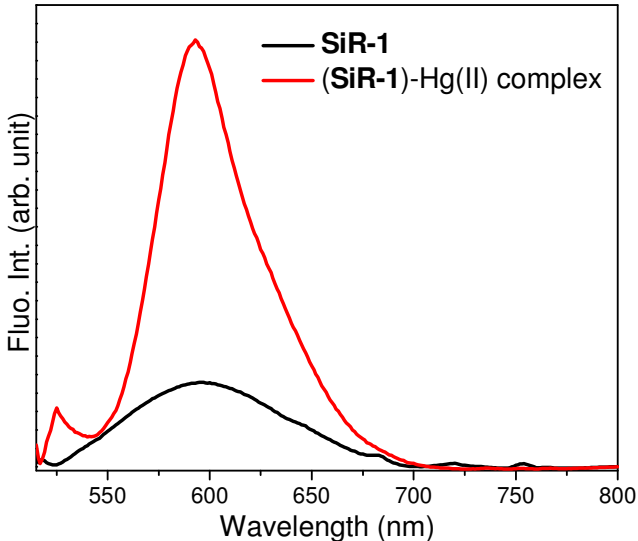


Fig. S17: Comparative fluorescence of **SiR-1** and **(SiR-1)-Hg(II)** complex in solid state, $\lambda_{\text{ex}} = 500$ nm, em. and ex. b. p. = 5nm, RT.

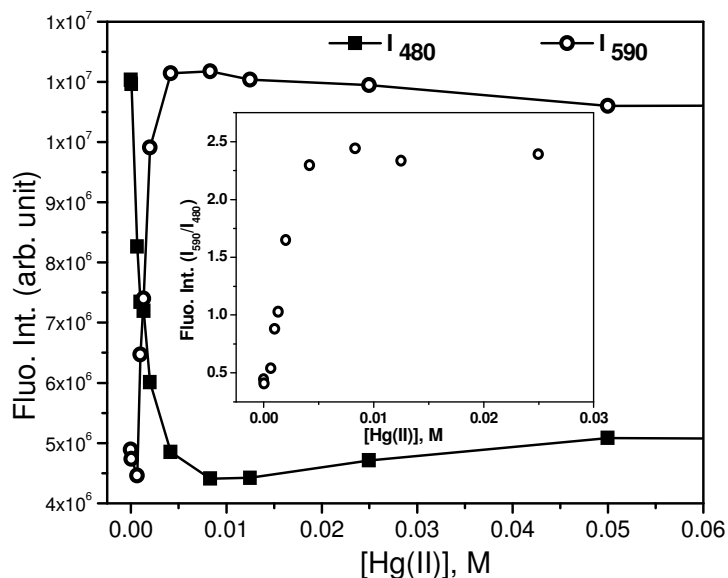


Fig. S18: Fluorescence spectral profile at 480nm and 590nm respectively and (Inset) corresponding ratiometric (I_{590}/I_{480}) signals of **SiR-1** suspension in aqueous medium upon addition of various concentration of Hg(II), $\lambda_{\text{ex}} = 400$ nm, em. and ex. b. p. = 5nm, RT.

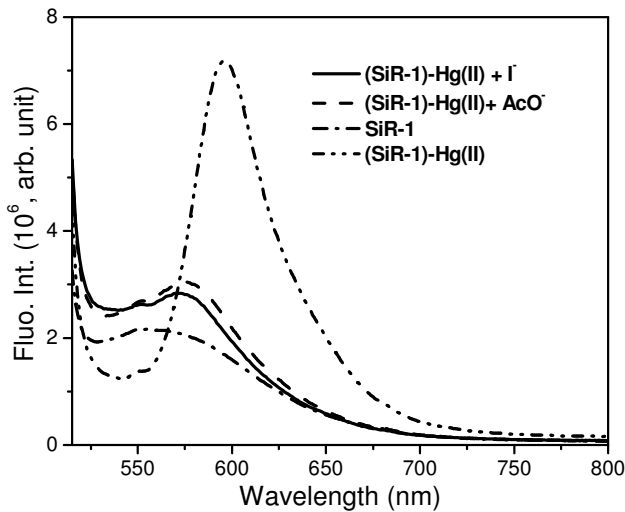


Fig. S19: Fluorescence spectra of (**SiR-1**)-Hg(II) upon addition of counter anions such as Γ (KI) and OAc^- (NH_4OAc) in aqueous medium, $\lambda_{ex} = 500$ nm, em. and ex. b. p. = 5nm, RT.

In a control experiment, fluorescence of Hg(II) complexed **SiR-1** was measured as a function of dilution of its dispersion in aqueous medium. The (**SiR-1**)-Hg(II) complex dispersed at higher concentration (>3 mM) has resulted in appearance of two new fluorescence peaks around 575nm and 625nm upon excitation at 500nm, which disappeared on subsequent dilution of the solution (Fig.S18) and showed a peak at 590nm. This may be due to formation of various excited state emissive interactions at higher concentration depending upon dispersion pattern, which vanishes on dilution. Nevertheless, the optical signal in form of sharp peak observed at 590nm at low concentration of in-situ formed complex facilitates chemosensing application.

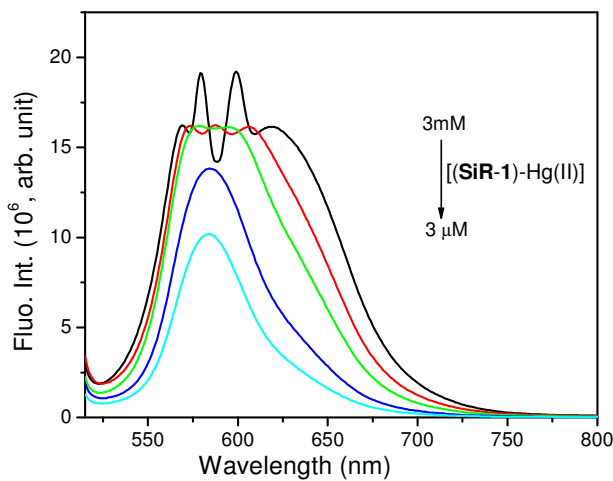


Fig. S20: Fluorescence spectra of **SiR-1**-Hg(II) complex at different dilutions in aqueous medium, $\lambda_{ex} = 500$ nm, em. and ex. b. p. = 5nm, RT.